ELSEVIER

7 October 1994

Chemical Physics Letters 228 (1994) 369-378

CHEMICAL PHYSICS LETTERS

Femtosecond pH jump: dynamics of acid–base reactions in solvent cages

Sang Kyu Kim [1], Juen-Kai Wang, Ahmed H. Zewail

Arthur Amos Noyes Laboratory of Chemical Physics [2], California Institute of Technology, Pasadena, CA 91125, USA

Received 19 July 1994; in final form 3 August 1994

Abstract

Studies are reported of the dynamics of proton-transfer reactions, with sub-picosecond time resolution, in solvent cages. The acid–base system studied in a molecular beam is 1-naphthol as a solute and ammonia (or water) as a solvent, with the number of solvent molecules (n) varying. At the threshold ($n=3$) for proton transfer we examine the accurate form of the decay, which has an apparent biexponential character, and we relate it to the nature of deprotonation and recombination. From studies of the effect of the total energy, isotope substitution and solvent number (n), we discuss the nature of the transfer and the interplay between the local structure of the base solvent and the dynamics.

1. Introduction

In bulk media, proton transfer in acid–base reactions is ubiquitous in chemistry and biology (for some reviews see Refs. [1-3]). Fundamental to this process are the energetics of the initial and final states and the dynamical structure of the solvent. Eigen and deMaeyer's early studies [4] of acid solutions provided the dissociation and recombination rates (hence, equilibrium constants) and proposed a local structure for the proton, $(H_9O_4)^+$, in water.

A key point in the measurements of the rates is the ability to induce an acid/base reaction on a relatively short time scale ('pH jump') and to follow the change with time. Förster [5] and Weller [6] showed that with light such instantaneous change of the pK_a can be studied by absorption to the excited state. Using a four-level description, the Förster cycle, one can deduce the energetics and changes in rates. With picosecond lasers, such reactions came under examination with new results on the fast rates and the effect of the solvent on them (see e.g., Refs. [2,3,7]).

For naphthols in water (and other solvents) the groups of Robinson and Clark [8] have studied the proton transfer in pure water and in mixed solvents; they reported 32 ps for pure water. Robinson proposed, based on these studies, that in water the hydration involves an instantaneous structure of 4 ± 1 water molecules, consistent with Eigen's suggestion. Because the experiments were conducted in the bulk, there was no direct evidence of such structures.

Some time ago we approached this problem by considering the effect of microscopic solvation in clusters of controlled size [9], and for 1-naphthol (referred to here as AH or 1-NpOH) we increased the degree of solvation by water or ammonia by using finite sized clusters of $AH \cdot (H_2O)_n$ or $AH \cdot (NH_3)_n$ in a molecular beam [10]. With picosecond resolution we found that the proton transfer is 'turned on' when n for ammonia changed to 3. In other words, three ammonia solvent molecules were sufficient for a sta-

[1] Arthur Amos Noyes Research Fellow.

[2] Contribution No. 8968.

0009-2614/94/$07.00 © 1994 Elsevier Science B.V. All rights reserved

SSDI 0009-2614(94)00951-1

ble structure of $A^-...H^+B_n$ to be formed. Thorough spectroscopic studies by Leutwyler's group [11] have shown red shifts and spectral broadening consistent with the change due to proton transfer for $n=4$. Syage et al., in a series of papers [12], have studied the phenol system and showed the applicability of the approach for the study of solvation effect in real time. With the addition of photoelectron detection it was possible to examine the solvent rearrangement. Kelley and Bernstein [13] studied the naphthol system and described a tunneling mechanism to account for the rates. In view of our work on the femtosecond dynamics of intramolecular proton transfer [14], we extend the earlier study of naphthol [10] to the femtosecond resolution of the elementary dynamics as the solvent number increases. For clusters, such resolution has been found to be crucial in the studies of the primary processes of fragmentation and ionization, as demonstrated by the groups of Castleman [15] and Gerber [16].

In this Letter, we report new studies of proton transfer dynamics at different total energies for the $AH...B_n$ and $AD...B_n$ systems; clusters of up to 20–30 solvent (B) molecules can be formed in the molecular beam. Our objective encompasses several points. First, in view of the relatively large uncertainty in the earlier measured rates (due to the picosecond resolution and the non-exponentiality of the decay) we wish to report here accurate measurements of the rates and the form of the decay, with sub-picosecond resolution. The long time behaviors have been obtained with a much better accuracy than the earlier work [10,13]. Second, the effect of total vibrational energy and isotope effect (H/D) may help us to unravel the dynamics of intramolecular vibrational redistribution (IVR) and tunneling. Third, the elementary steps of dissociation, recombination, and solvent rearrangement could be separated, especially because sub-picosecond time resolution is sufficiently short.

The system under study is generally bimolecular in solutions,

$$A^*H + B_n \rightleftharpoons A^{-*}...H^+B_n\,. \qquad (1)$$

In the solvent cage,

$$A^*H...B_n \rightleftharpoons [A^{-*}...H^+B_n]_u \rightarrow [A^{-*}...H^+B_n]_e\,, \qquad (2)$$

the system defines sharply the processes involved as it changes from the unequilibriated (u) to equilibriated (e) structures. Because of the weak hydrogen bond, the zero-of-time can be defined, similar to other studies of bimolecular reactions in real time [17–19], and the diffusion-controlled processes are eliminated. With the time resolution reported here, the acidity is initiated with the femtosecond pulses resulting in a very large change in pK_a (femtosecond pH jump; the meaning of a pH for the cluster is of course somewhat different from bulk); AH has a pK_a of 9.4 and A*H of 0.5 [20]. Finally, the reversible process in Eq. (2) is due to a finite number of solvent molecules around the solute, miscible or immiscible [21], and the conventional kinetics approach may become inapplicable. In bulk studies Huppert, Pines and Agmon [22], and Pines and Fleming [23] have shown the effect of reversibility on the time-dependent form associated with Eq. (1).

The potential energy surface is normally thought of as a simple double well, Fig. 1. This is because the hydrogen bond is relatively weak and the configurations A*H and H^+B_n are much different. Accordingly, the problem is reduced to an effective potential with the rates being determined by the residence time on A*H or by the frequency of going between the two minima. If tunneling is the dominant mechanism, then the time for transfer will depend on the nature

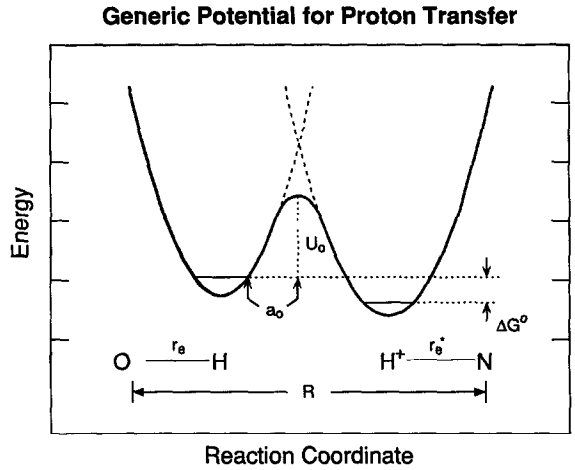

Fig. 1. Generic potential of proton-transfer reactions. The barrier height is U_0 and the half width along the reaction coordinate (q) is a_0. Tunneling rates depend on U_0 and a_0. R is defined as the distance between O and N atoms of 1-naphthol and ammonia, respectively. The reaction coordinate for this case is the motion of the proton between two potential minima.

of the potential (barrier height and width) and the effective mass. For example, with a width of ≈0.5 Å and a barrier height of ≈3 kcal/mol, the time is a few picoseconds. As shown by Ando and Hynes [24] the final transfer may involve several steps on going from 'contact' to 'solvent-separated' ion pairs; tunneling may not be as simple as the picture in Fig. 1 implies. On this time scale of picoseconds one must consider the role of IVR in the initial transfer and after the transfer. The latter has been shown to be essential in intramolecular hydrogen-atom transfer [14]. In addition, solvent fluctuation and reorganization may or may not influence such redistribution depending on the time scale. Here, we address these issues and examine the nature of the reaction coordinate.

2. Experimental

The experimental details will be given elsewhere. Briefly, a tunable femtosecond synchronously pumped dye laser system and its associated pulsed dye amplifier produced ≈500 μJ laser pulses at 614 or 640 nm. After a prism-pair compressor, the amplified laser pulses were split into two parts. One was sent to another pulsed dye amplifier to boost its energy, passed through a computer-controlled time delay line, and was then focused into a doubling crystal (KDP) to generate the pump pulses at 307 or 320 nm. The other part of the laser pulse was focused into a water cell to generate a super-continuum. From this super-continuum, a 10 nm band-pass interference filter was used to select a wavelength of 680 or 740 nm. The selected radiation was amplified in a pulsed dye amplifier, and the amplified beam was focused into another KDP crystal to produce the probe pulses at 340 or 370 nm. The pump and probe laser beams were subsequently recombined and focused into the skimmed molecular beam (Fig. 2). The pulse width of our system is generally as short as ≈100 fs, but for these experiments we fit the rise to ≈600 fs as an operational procedure for handling the decay characteristics at longer times.

The beam was prepared by heating a sample of 1-naphthol (Kodak) to 100±20°C and seeding it in a pre-mixed carrier gas of NH_3 and He (0.5% of NH_3 in He) with a backing pressure of 30–40 psi. For the deuterium effect experiment, 1-NpOH in ether was washed with D_2O several times, separated, and collected [13]. To avoid exchange, deuterated ammonia (ND_3) in He was used as the carrier gas. The mixture was then expanded through a pulsed nozzle (0.25 mm diameter) into a vacuum chamber to generate 1-naphthol–ammonia clusters. The resulting cluster beam passed through a 2 mm skimmer into a second chamber (maintained at $\approx 5\times10^{-7}$ Torr) and crossed with the focused laser beams for time-of-flight (TOF) mass spectrometry.

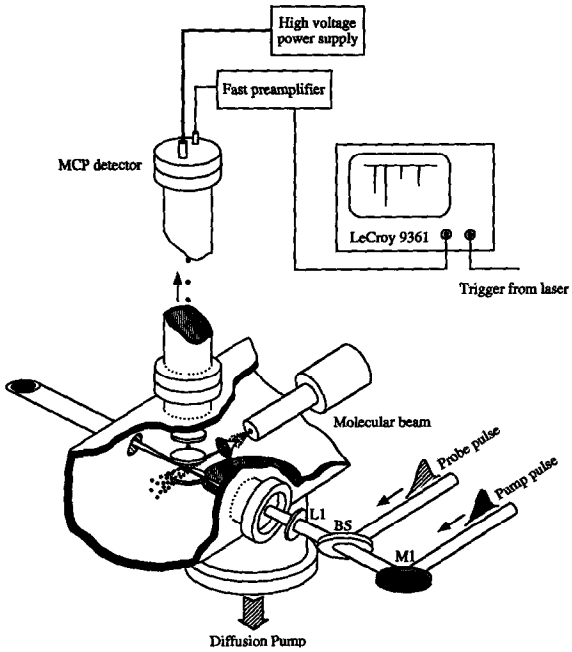

Fig. 2. Schematic of the experimental arrangement showing the time-of-flight (TOF) mass spectrometry and the two laser pulses used. The pump and probe laser beams are focused at the skimmed molecular beam. BS: beam splitter; L1: focusing lens; M1: mirror.

Using the two-pulse configuration, the mass spectra were collected by a fast digital oscilloscope (LeCroy 9361). The ion signal for a specific mass unit was selected by a gated integrator (SR250), and monitored as a function of the delay time between pump and probe pulses to give the transient for a specific cluster. The transients were averaged over 10 laser shots and 40–60 scans, typically reaching a signal-to-noise ratio of 20 or more. This allowed us to reproduce the non-exponential behavior and to obtain accurate fits. We checked for the linearity of the pump–power dependence; the probe power was very weak.

3. Results and discussion

The TOF mass spectrum for 1-NpOH·$(NH_3)_n$ clusters obtained with a laser wavelength of 320 nm is shown in Fig. 3. Clusters as large as $n=30$ were formed in the molecular beam. The transients for A*H with $n=3$ and A*D with $n=3$, taken at two different pump energies, are shown in Fig. 4. These transients show distinct biexponential decays and were fit with a function of the form, $S[t]=A_0[R\exp(-t/\tau_1)+\exp(-t/\tau_2)]$, which was convoluted with the instrumental response function. The results of the fits for $n=3$ and 4 clusters are listed in Table 1.

Transients were also obtained for $n=0$ to $n=6$ and the results are shown in Fig. 5. The transients for $n=0$–4 were taken at 320/340 nm (pump/probe), while those for $n=5$ and 6 were obtained at 320/370 and 326/370 nm, respectively. With the 320/340 nm arrangement no time-dependent signal was observed for clusters larger than $n=4$, possibly due to ion fragmentation [12]. The transients for clusters of $n=3$, 4, and 5 show an initial fast decay, while the others show relatively slow decay with time constants of tens of nanoseconds, which are comparable to the fluorescence lifetimes of the excited state [10]. A very fast initial decay with small amplitude was observed within the first few picoseconds for the $n=5$ transient.

3.1. Structure

The structure of clusters formed in a molecular beam is quite important in determining the energetics and dynamics of the proton transfer reaction. Felker's group, using rotational coherence spectroscopy, has shown that for the 1:1 complex, the NH_3 is attached to the OH group of 1-NpOH by forming a H bond between the (O–)H and N atoms [25]. Pratt's group [26] obtained the structure for the 2-NpOH/ammonia complex from high-resolution spectra; the structure is similar to that of 1-NpOH, with slightly different interatomic distances. Bernstein and coworkers [27] have calculated the most probable structure for the 1:1 complex as the one in which NH_3 resides on the ring of 1-NpOH. For the $n=2$ cluster, there are two geometrical isomers for which distinct spectral origins have been observed. Felker's group found that both NH_3 molecules are attached to the OH group in one geometrical isomer, while for the other isomer the results were suggestive of an NH_3 bound to the ring of 1-NpOH.

For the $n=3$ cluster, several geometrical isomers

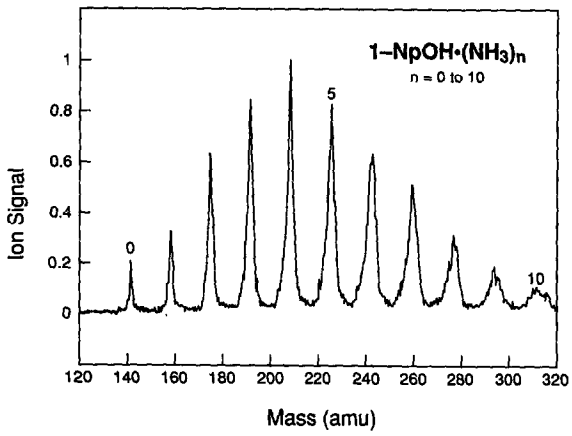

Fig. 3. Time-of-flight mass spectrum of the naphthol–ammonia molecular beam ($\lambda=320$ nm).

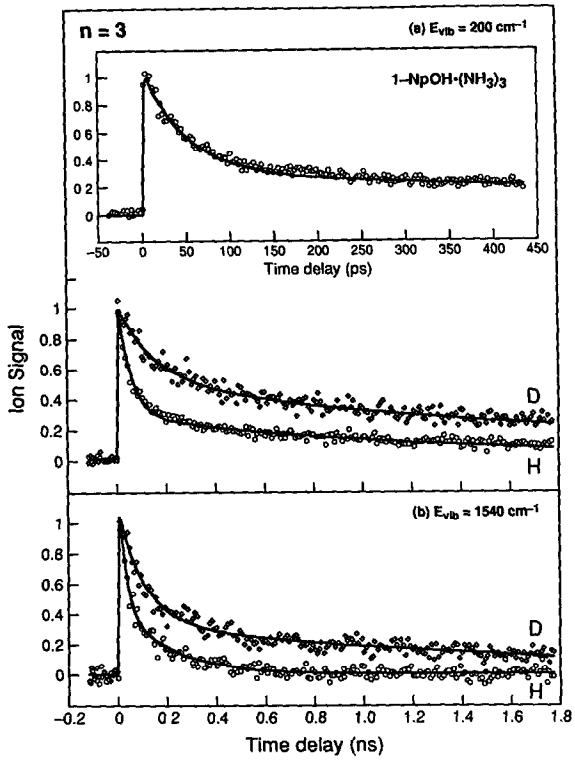

Fig. 4. Experimental transients and theoretical fits for 1-NpOH·$(NH_3)_3$ and 1-NpOD·$(ND_3)_3$: (a) pump/probe wavelengths of 320/340 nm and (b) at 307/340 nm. Excess vibrational energies are calculated relative to the origin at 31050 cm^{-1} for $n=3$ cluster.

Table 1
Biexponential fits to observed transients [a]

		320 nm			307 nm		
		τ_1	τ_2	R	τ_1	τ_2	R
$n=3$	H	52 (4)	1210 (60)	2.5	25 (3)	226 (20)	2.2
	D	150 (20)	>2100	1.0 [b]	100 (10)	1720 (150)	2.1
$n=4$	H	93 (8)	>2700	0.6 [b]	70 (6)	727 (25)	0.8
	D	335 (200)	>8000	0.4 [b]	152 (35)	>5000	0.4 [b]

[a] τ_1 and τ_2 are in ps. The values in parentheses are standard deviations. The uncertainty of R, which is defined in the text, is within 20%–30%.
[b] Less reliable due to large uncertainties of τ_2.

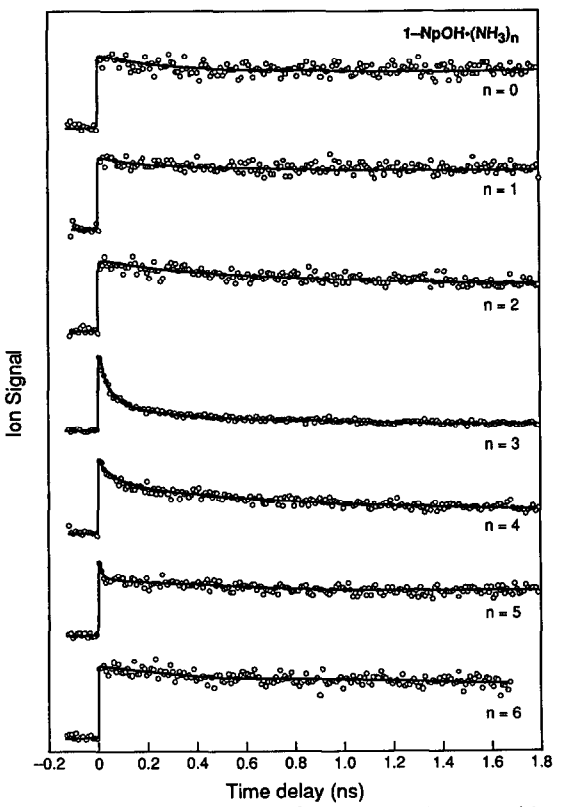

Fig. 5. Experimental transients for 1-NpOH·$(NH_3)_n$; with n varying from 0 to 6. Pump/probe wavelengths are as follows: 320/340 nm for $n=0$–4; 320/370 nm for $n=5$; and 326/370 nm for $n=6$.

are possible. Felker's group found that at least one of the conformers, which corresponds to the relatively sharp spectral origin, has a structure in which all three NH_3 molecules are attached to the OH group of 1-NpOH. Because of the sharpness of the spectra, this structure was assigned to the conformer where no proton transfer took place. Even for the $n=3$ cluster, because of the spectral congestion caused by proton transfer, Felker's group could not determine the structure of clusters which undergo proton transfer. As discussed below, some ammonia molecules may reside on the ring and affect the energetics involved in the proton transfer dynamics, thus establishing an interplay between the structure and the dynamics.

3.2. Energetics

The change of pK_a from 9.4 in the ground state to 0.5 in the excited state [20] reduces the enthalpy of deprotonation, ΔH_d, by ≈ 12 kcal/mol to give $\Delta H_d \approx 327$ kcal/mol in the excited state [11]. Solvent molecules $(NH_3)_n$ in the cluster, through hydrogen bonding, give a stabilization energy for neutral A*H of $\Delta H_{stab} \approx 14$ kcal/mol for $n=3$ [28]. The proton affinity, PA_n, of $(NH_3)_n$ and the electrostatic stabilization energy, V_n, of the ion-pair product state of $A^{-*}...H^+B_n$ contribute to the overall stabilization of the newly formed acid–base complex. Therefore, the enthalpy of the proton transfer reaction, $\Delta H_{PT}(n)$, for $A^*H(NH_3)_n$ is given by

$$\Delta H_{PT}(n) = [\Delta H_d + \Delta H_{stab}(n)] - (PA_n + V_n), \quad (3)$$

where, for simplicity, the absolute values are used for all terms except for $\Delta H_{PT}(n)$.

To determine V_n the charge densities of atoms in the cluster must be known. However, V_n can be estimated in the following way. Because the threshold size for proton transfer in $A^*H\cdot(NH_3)_n$ is $n=3$ and the

proton affinity of $(NH_3)_3$ is ≈ 238 kcal/mol [11], it follows from Eq. (3) that V_3 should be equal to or larger than ≈ 103 kcal/mol. For the reaction to proceed, $\Delta H_{PT}(n=3)$ is taken to be equal or less than zero. Once the acid–base complex is formed, solvent reorganization is expected to occur to further stabilize the ion-pair product states, as discussed below.

3.3. Dynamics

We first consider the most elementary steps that could be involved in the transfer and solvation. Since the observed rates are much slower than those characteristic of coherent wave-packet motion [29], we shall use rate processes to describe the system outlined in Eq. (2),

$$A^*H...B_n \underset{k_{-1}}{\overset{k_1}{\rightleftharpoons}} [A^{-*}...H^+B_n]_u \xrightarrow{k_2} [A^{-*}...H^+B_n]_e . \tag{4}$$

It follows that by monitoring $A^*H...B_n$ alone a biexponential decay would be observed. The fast component is determined by $\approx (k_1+k_{-1})$ while the slow component reflects the effect of k_2 process. It is important to realize that Eq. (4) in the absence of the k_{-1} process can give rise to an apparent biexponential decay if both $A^*H...B_n$ and $[A^{-*}...H^+B_n]_u$ are assumed to be detectable with different ionization cross sections; a ratio around 1:0.1–0.3 for $A^*H...B_n$ and $A^{-*}...H^+B_n$ can be invoked. In this case, the fast and slow decays represent the proton transfer and solvent reorganization rate, respectively, and the ratio of fast to slow decays represents the relative ionization cross sections. The transient for 1-NpOH·$(NH_3)_3$ at 307 nm (where $k_2^{-1} \approx 150$ ps) decays to zero background (Fig. 4), suggesting that the final product, $[A^{-*}...H^+B_n]_e$, is not detectable since one expects for this species a rise with a plateau.

In Table 2, we present the fit parameters to the biexponential form given by Eq. (4). We note, from Table 2, that the fast rate of transfer is very sensitive to the isotopic substitution and to the total energy, consistent with the trends given in Ref. [13]. However, the results in Ref. [13] are quantitatively different from ours. For example, for the $n=3$ cluster, our fast decay component (from Table 1) is 52 ± 4 ps while the slow component is 1210 ± 60 ps. The results in Ref. [13] gave 57 ± 15 and 440 ± 125 ps, respectively. The slow component is crucial to the form of the decay and to the possible inaccuracies introduced in the fitted values of Refs. [10,13].

Table 2
The $n=3$ system: k_1, k_{-1} and k_2 [a]

E_{vib} (cm^{-1}) [b]	Time (ps)	$n=3$	
		H	D
200	$1/k_1$	71 (9)	275 (40)
(320 nm)	$1/k_{-1}$	200 (40)	370 [c]
	$1/k_2$	910 (60)	>1120
1540	$1/k_1$	35 (4)	143 (10)
(307 nm)	$1/k_{-1}$	106 (30)	357 (90)
	$1/k_2$	164 (25)	1200 (170)

[a] Rate constants are obtained from time constants and ratios listed in Table 1 using the following relations: $1/\tau_1+1/\tau_2=k_1+k_{-1}+k_2$, $1/\tau_1\tau_2=k_1k_2$, and $R=(\alpha+k_1-k_{-1}-k_2)/(\alpha-k_1+k_{-1}+k_2)$, where $\alpha=\sqrt{(k_1+k_{-1}+k_2)^2-4k_1k_2}$.
[b] Vibrational energies were calculated relative to the origin at 31050 cm^{-1} for $n=3$ cluster (see Refs. [11,27]), and they represent the average values at the center of our excitation pulses.
[c] Less reliable due to uncertainties of values in Table 1.

With the sub-picosecond resolution reported here, we observed no faster decay than the picosecond value given for $n=3$. From Table 2, it is apparent that k_1 increases with the total energy and decreases with D substitution. The value of k_{-1} is consistently smaller than that of k_1, and on the time scale of both k_1 and k_{-1} IVR may play a role. The IVR rate is expected to become faster as the density of states increases in 1-NpOH itself [30] or due to cluster modes [31]. Hence, increasing the vibrational energy, decreasing the vibrational frequencies by H/D isotopic substitution, or increasing the number of degrees of freedom by increasing the number of solvent molecules should increase the rate constant of IVR. The time constants listed in Table 1 show that neither τ_1 nor τ_2 is consistent with the above trend except for vibrational energy. Moreover, some of our measurements were made near the origin where one expects IVR to be on a very long time scale. Accordingly, our scheme in Eq. (4) does not include an IVR process, although it is part of the description of the solvent reorganization. We now consider the different steps involved.

3.3.1. Proton transfer by tunneling

The mechanism of proton transfer has been extensively modeled and studied (see e.g. Refs. [1–3,13,32]). There are mainly three coordinates to be considered: the motion of the proton along the reaction coordinate (q), the vibration of O and N atoms of 1-naphthol and ammonia, respectively, along the intermolecular coordinate (Q), and the motion of solvent molecules along the solvent coordinate (S). In clusters, the solvent configuration at early times may be fixed. Accordingly, the proton transfer may be described as tunneling along the q coordinate through the barrier, with the height and width being modulated by the O–N van der Waals stretch motion along the Q coordinate.

Generally, the semi-classical expression for the tunneling rate constant from bound-to-free (inverted) parabolic potential energy surfaces is given by [1]

$$k = \nu \exp\left(-\frac{a_0}{\hbar}\pi\sqrt{2mU_0}\right), \tag{5}$$

where ν is the OH vibrational frequency, m is the effective mass, a_0 is the half width of the barrier, and U_0 is the barrier height (see Fig. 1). U_0 and a_0 are strongly modified by the O–N stretching vibrational motion, and these effects can be considered by calculating an expectation value of tunneling rate constant for each quantum state of the O–N stretch [13]. For example, at the origin, k in Eq. (5) should be averaged over the zero-point vibrational motion of the O–N stretch, $k_0 = \langle \phi_0 | k | \phi_0 \rangle$, where ϕ_0 is the harmonic wavefunction for the O–N stretch mode at $v=0$. This dependence has been used to account for the trends in the experimental observations in Ref. [13]. The barrier width can be estimated from the structural studies which give the O–N distance to be in the range of 2.6–2.8 Å [25,26]. From a consideration of the classical turning points of zero-point vibrations of OH and NH, the half width of the barrier at the zero-point vibrational energy level of the reactant is in the range of 0.2–0.3 Å. With $a_0 = 0.3$ Å and $k_0 = 50$ ps^{-1}, the barrier height is deduced to be ≈ 2000 cm^{-1} (≈ 8000 cm^{-1} if $a_0 = 0.2$ Å is used).

The decrease of the rates with D substitution combines the three characteristics of the isotope effect: the change of the mass, the change in the zero-point energy, and the change of the frequency. The tunneling model is consistent with this change of the rates. With the same model Kelley and Bernstein et al. [13] could account qualitatively for the energy dependence by assuming that the energy is statistically channeled into the reaction coordinate. It is of course not necessary to assume complete redistribution, as the key here is the probability of being in the reactive coordinate which increases with energy. Syage [12] introduced a bound-to-bound tunneling model, which includes the low-frequency O–N stretch and solvent motions, to quantify the results of the phenol and naphthol systems.

The simple tunneling model seems to give a global description of the process, but it does not address some important issues underlying the dynamics. First, the reaction coordinate is surely not that simple. In fact in studies of intramolecular proton transfer [14,33,34], the reaction coordinate is shown to involve low-frequency modes and not the OH stretch vibration. In the intermolecular proton-transfer case the reaction coordinate is coupled to the solvent coordinate as one knows that solvent reorganization must take place. Second, from a molecular dynamics point of view, it is not clear that the proton transfer involves only one step. In fact, the study by Ando and Hynes [24] of HCl in water shows a two-step process for the creation of the 'contact' and 'solvent-separated' ion pairs. Tunneling was shown to be insignificant in the first step [24]. It would be interesting to follow the proton-transfer dynamics of the system under study here with molecular dynamics simulations in clusters of different sizes. This would allow us to examine the motion of the individual solvent molecules involved, eventually reaching the dielectric continuum limit in bulk. This work is currently in progress in collaboration with the Hynes group.

3.3.2. Structures and dynamics: size dependence

The number of solvent molecules is important to the energetics of proton transfer. As the number of solvent molecules increases, PA_n increases. V_n is expected to decrease due to the increase in dielectric shielding, causing delocalization of the positive charge of the ion-pair state by solvent molecules adjacent to the proton. Hence, depending on the change of each term with n, $PA_n + V_n$ could have a maximum as a function of solvent number. A maximum in the proton-transfer rate constant might follow.

The structure of the cluster could also be a significant factor; it determines the energetics, since both PA_n and V_n are closely related to the geometrical structures of the cluster. As mentioned earlier, there could be two geometrical isomers (I and II) for $n=3$ clusters; I has a structure in which all three NH_3 molecules are on the side of the OH group and II has a structure in which two NH_3 molecules are attached to the OH group and one NH_3 resides on the ring. As pointed out by Felker's group [25], V_n of I is expected to be smaller than that of II since the dielectric shielding is likely to be more effective for I than II. Therefore, from Eq. (3), structure II would be more favorable for proton transfer than I assuming that the proton affinity remains similar; the stability will depend on the net change in PA_n and V_n upon changing the NH_3 position. This indicates that the energetics and dynamics of proton transfer are critically dependent on the structure. This point is significant even in bulk studies, as discussed in Section 1.

Studies have also been made in clusters with various other solvents such as water and piperidine. Proton transfer has not been observed for clusters with $(H_2O)_n$ of $n \leqslant 20$ [10,11], while it has been observed for clusters with piperidine and ammonia of $n=2$ and 3, respectively [10]. Considering the proton affinity of solvent molecules, the threshold for proton transfer is estimated to be at $n=30$–50 for clusters with water [11]. But no proton transfer has been observed in bulk ice [11]. Recently, proton transfer has been observed for clusters with $(H_2O)_n$ of $20 \leqslant n \leqslant 800$ [35]; the time scale is much longer (0.5–1.5 ns) than that found in water solution. In the bulk solution, the solvent reorganization is easier, and this may account for the disparity in time scales (32 ps versus 0.5–1.5 ns) and the inefficiency of the transfer in ice.

The size dependence of the dynamics is quite dramatic (Fig. 5). The proton-transfer rate constant for $n=4$ cluster is smaller than that of $n=3$. This trend is consistent with the findings of Eq. (4). The forward reaction is ≈ 3 times faster than the reverse reaction for $n=3$, which means that the reaction is exothermic, giving a negative ΔG^0. For $n=4$, the ratio of k_1 and k_{-1} is nearly 1, giving ΔG^0 of nearly zero. The sharp initial decay observed for $n=5$ could be consistent with a continued increase in k_{-1}, giving the small $\approx 20\%$ amplitude. (Note that the excess vibrational energy is larger for the larger clusters and the decay is expected to be faster.)

The above trend suggests that the solvent configuration for clusters formed in the molecular beam may become more favorable for reactants compared to products as cluster size increases. As discussed before, the hydrogen-bonded structure determines the stability of charge separation. Based on the proton affinity factor *alone* the experimental results cannot be explained; PA for $n=4$ is larger than PA for $n=3$, and we expect a faster rate for $n=4$. But there are other possibilities. For example, for clusters larger than $n=4$, proton transfer might occur even in the ground state, and the transients for $n=5$ and 6 clusters in Fig. 5 may be due to the significant contribution from ion-pair states in the ground state. Another possibility is passage through the Marcus inverted region, where the absolute value of ΔG^0 exceeds the solvent reorganization energy. In other words, as the number of solvent molecules increases, the free energy difference exceeds the solvent reorganization energy, resulting in an increase in the activation energy. Hence a smaller rate constant [12]. This description is based on the assumption that strong solvation is the driving force of the proton transfer reaction.

3.3.3. Solvent reorganization

In the model discussed above, k_2 (Table 2) is related to the irreversible processes of equilibration which involve fragmentation, IVR, emission, or solvent reorganization. If fragmentation is one of the processes, then the product would be the $NH_4^+ \cdot (NH_3)_{n-1}$ complex. But, in contrast to the case of phenol–$(NH_3)_n$ complex [12], no ammonia complex could be detected in this work. The lifetime of emission has been measured to be tens of nanoseconds [10], and therefore this process is excluded. Accordingly, the slow decay time in transients is associated with solvent reorganization which includes IVR in the product form. The ion-pair complex is formed on the picosecond time scale, and the solvent rearrangement takes place for further stabilization of acid–base product state. The reorganization requires the dissociation and formation of hydrogen bonds as well as the 'rotation' of solvent molecules. In the clusters at low temperatures, the time scale for solvation is therefore expected to be slower compared to that in bulk media. Recent time-resolved photoelectron

spectroscopic studies showed that the time constant for solvent reorganization in phenol–ammonia clusters is around 300 ps [12].

The dependence of τ_2 or $1/k_2$ on vibrational energy, cluster size, and H/D isotope substitution is quite noticeable (see Tables 1 and 2). As the total vibrational energy increases, the intermolecular vibrational motions are increasingly excited, thus facilitating the solvent motion, hence leading to an increase in the rates. As the cluster size gets larger, the number of intermolecular modes associated with solvent motions increase. The solvent reorganization along a specific coordinate is accordingly expected to be slower as the probability of populating this coordinate decreases with the number of modes increasing. The effect of H/D isotope substitution on τ_2 or $1/k_2$ is large and this suggests the involvement of the intermolecular modes. The solvation energies associated with solvent motions are not accurately known, and, therefore, one cannot rule out the possibility of the existence of structural isomers which undergo different (or no) proton-transfer dynamics. As discussed before, the reaction coordinate must involve the solvent motions and the local structure of the solvent is therefore critical.

4. Conclusion

We considered in this study the nature of proton transfer reactions in acid–base systems of clusters of 1-naphthol and ammonia (or water). Solvent number dependence was examined by varying the cluster size in a molecular beam. Accurate forms of the transients observed with sub-picosecond resolution indicated the time scale for deprotonation, recombination, and solvent reorganization. With a simple model, we considered the dynamics of tunneling, the reaction coordinate, and the interplay between solvent structure and dynamics of the transfer. Future theoretical work is planned for addressing the molecular dynamics of these finite-sized systems in comparison with bulk reactions.

Acknowledgement

The helpful discussions with Dr. J.A. Syage, and Professor P.M. Felker, Professor E.R. Bernstein, and Professor M. Okumura are greatly appreciated. We wish to also thank the referee for the valuable suggestions, and Mr. Q. Liu and A. Heikal for their help. This work was supported by a grant from the National Science Foundation.

References

[1] R.P. Bell, The proton in chemistry (Chapman and Hall, London, 1973); The tunnel effect in chemistry (Chapman and Hall, London, 1980).
[2] P.F. Barbara and H.P. Trommsdorff, eds., Chem. Phys., Special issue 136 (1989) 153;
V.A. Benderskii, V.I. Goldanskii and J. Jortner, eds., Chem. Phys., Special issue 170 (1993) 265;
N. Agmon and R.D. Levine, eds., Chem. Phys., Special issue 183 (1994) 167.
[3] P.F. Barbara, G.C. Walker and T.P. Smith, Science 256 (1992) 975;
G.J. Kearley, F. Fillaux, M.H. Baron, S. Bernnington and J. Tomkinson, Science 264 (1994) 1285.
[4] M. Eigen and L. deMaeyer, in: The structure of electrolytic solutions, ed. W.J. Hamer (Wiley, New York, 1959), and references therein.
[5] T. Förster, Naturwissenschaften 36 (1949) 186; Z. Elektrochem. 54 (1950) 531.
[6] A. Weller, Z. Elektrochem. 56 (1952) 662.
[7] P.M. Rentzepis and P.F. Barbara, Advan. Chem. Phys. 87 (1981) 627;
E.M. Kosower and D. Huppert, Ann. Rev. Phys. Chem. 37 (1986) 127.
[8] J. Lee, G.W. Robinson, S.P. Webb, L.A. Phillips and J.H. Clark, J. Am. Chem. Soc. 108 (1986) 6538, and references therein.
[9] P.M. Felker and A.H. Zewail, Chem. Phys. Letters 94 (1983) 448, 454; J. Chem. Phys. 78 (1983) 5266.
[10] J.J. Breen, L.W. Peng, D.M. Willberg, A. Heikal, P. Cong and A.H. Zewail, J. Chem. Phys. 92 (1990) 805.
[11] O. Cheshnovsky and S. Leutwyler, J. Chem. Phys. 88 (1988) 4127;
R. Knochenmuss and S. Leutwyler, J. Chem. Phys. 91 (1989) 1268.
[12] J. Steadman and J.A. Syage, J. Chem. Phys. 92 (1990) 4630; J.A. Syage, J. Phys. Chem. 97 (1993) 12523; Z. Physik D 30 (1994) 1, and references therein.
[13] M.F. Hineman, G.A. Brucker, D.F. Kelley and E.R. Bernstein, J. Chem. Phys. 97 (1992) 3341.
[14] J.L. Herek, S. Pedersen, L. Bañares and A.H. Zewail, J. Chem. Phys. 97 (1992) 9046.
[15] S. Wei, J. Purnell, S.A. Buzza, R.J. Stanley and A.W. Castleman Jr., J. Chem. Phys. 97 (1992) 9480.
[16] T. Baumert, M. Grosser, R. Thalweisser and G. Gerber, Phys. Rev. Letters 67 (1991) 3753.
[17] N.F. Scherer, L.R. Khundkar, R.B. Bernstein and A.H. Zewail, J. Chem. Phys. 87 (1987) 1451.

[18] S.I. Ionov, G.A. Brucker, C. Jaques, L. Valachovic and C. Wittig, J. Chem. Phys. 99 (1993) 6553.
[19] S.A. Wright, M.F. Tuchler and J.D. McDonald, Chem. Phys. Letters 226 (1994) 570.
[20] C.M. Harris and B.K. Selinger, J. Phys. Chem. 84 (1980) 1366.
[21] R.N. Pribble and T.S. Zwier, Science 265 (1994) 75.
[22] D. Huppert, E. Pines and N. Agmon, J. Opt. Soc. Am. B 7 (1990) 1545.
[23] E. Pines and G.R. Fleming, Chem. Phys. 183 (1994) 393.
[24] K. Ando and J.T. Hynes, in: Structure, energetics, and reactivity in aqueous solution, eds. C.J. Cramel and D.G. Truhlar, in press.
[25] L.L. Connell, Ph.D. Thesis, University of California, Los Angeles (1992).
[26] D.F. Plusquellic, X.-Q. Tan and D.W. Pratt, J. Chem. Phys. 96 (1992) 8026.
[27] S.K. Kim, S. Li and E.R. Bernstein, J. Chem. Phys. 95 (1991) 3119.
[28] N. Mikami, A. Okabe and I. Suzuki, J. Phys. Chem. 92 (1988) 1858;
S.T. Ceyer, P.W. Tiedeman, B.H. Mahan and Y.T. Lee, J. Chem. Phys. 70 (1979) 14.
[29] A.H. Zewail, Femtochemistry–ultrafast dynamics of the chemical bond (World Scientific, Singapore, 1994), and references therein.
[30] C. Lakshminarayan and J.L. Knee, J. Phys. Chem. 94 (1990) 2637.
[31] C. Lienau, A. Heikal and A.H. Zewail, Chem. Phys. 175 (1993) 171.
[32] D.C. Borgis and J.T. Hynes, Chem. Phys. 170 (1993) 315.
[33] T. Elsässer, in: Femtosecond chemistry, eds. J. Manz and L. Wöste (VCH Publishers, Weinheim, 1994).
[34] Th. Arthen-Engeland, T. Bultmann, N.P. Ernsting, M.A. Rodriguez and W. Thiel, Chem. Phys. 163 (1992) 43.
[35] R. Knochenmuss, G.R. Holtom and D. Ray, Chem. Phys. Letters 215 (1993) 188.